Progress In Electromagnetics Research C, Vol. 130, 15–30, 2023

Damping System for an Optimized Rotation Magnetized Direction Permanent Magnet Thrust Bearing

Amarsh Jalaik[1], Supreeth D. Kumar[1], Gireesha R. Chalageri[2, 3], Siddappa I. Bekinal[1, *], Mrityunjay Doddamani[4], and Shivamurthy R. Chandranna[1]

Abstract—An eddy current damper for an optimized rotation magnetized direction (RMD) permanent magnet thrust bearing (PMTB) was analyzed in this paper. Initially, the optimization of critical design variables was performed for a particular bearing volume for maximum force as well as stiffness. Then, generalized curve fit equations were established to obtain a correlation between different geometrical parameters concerning the outer diameter and air gap. Furthermore, the axial force of the optimized RMD configuration calculated using a mathematical model was validated using the results of FEA in ANSYS. Finally, finite element simulation was performed to evaluate the damping forces generated by an eddy current damper (ECD) for an optimized thrust bearing. Analysis has shown that eddy current dampers can improve system damping.

Nomenclature

AMB	Active magnetic bearing
Br	Magnetic flux density
$D1$	The inner diameter of rotor rings
$D2$	The outer diameter of rotor rings
$D3$	The inner diameter of the stator rings
$D4$	The outer diameter of the stator rings
ECD	Eddy current damper
f	Polarized faces of the stator
FEA	Finite element analysis
$F_{z\,\max}$	Maximum axial force
g	Number of surface elements on the stator faces
g	Air-gap
h	The axial thickness of rings
$K_{z\,\max}$	Maximum axial stiffness
L	Length of the bearing
m	Discrete elements on the faces of the magnet rings
n	Number of rings
Opt	Optimum
p	Number of rotor rings
PMB	Permanent magnet bearing
PMTB	Permanent magnet thrust bearing

Received 14 December 2022, Accepted 3 February 2023, Scheduled 16 February 2023

* Corresponding author: Siddappa Iranna Bekinal (siddappa.bekinal@manipal.edu).

[1] Department of Mechanical and Industrial Engineering, Manipal Institute of Technology, Manipal Academy of Higher Education, Manipal, Udupi, Karnataka 576104, India. [2] School of Mechanical Engineering, KLE Technological University, Hubballi, Karnataka 580031, India. [3] Visvesvaraya Technological University, Belagavi, Karnataka 590018, India. [4] School of Mechanical and Materials Engineering, Indian Institute of Technology Mandi, Mandi, Himachal Pradesh 175075, India.

q	Number of stator rings
RMD	Rotation magnetized direction
RMDPMTB	Rotation magnetized direction permanent magnet thrust bearing
t	Polarized faces of the rotor
w	Number of surface elements on the faces of the rotor

1. INTRODUCTION

Magnetic bearings are a class of bearings that provide contactless suspension of the rotor while exploiting the force generated due to magnets. A magnetic bearing is an alternative to conventional bearings. It has several advantages, including friction-free operation, lubrication-free operation, and no mechanical wear [1]. Magnetic bearings are classified into two types: active and passive. AMB is a class of magnetic bearings that employ sensors that assist in the levitation of the rotors [2]. But the use of sensors makes the system cumbersome and complicated. Hence, passive magnetic bearings can be employed because they provide non-contact suspension of the rotor without the aid of any sensors. A PMB is the most common type of passive magnetic bearing. Cost and size constraints make them attractive for high-speed applications. The stiffness and force generated by a single-ring PMB are very low but can be increased by adding multiple numbers of rings.

The force and stiffness for monolithic and multi-ring [3–6] PMB have been determined by Amperian and Coulombian models. Even though PMBs have attractive characteristics, they suffer from instability and poor damping. The stability of a PMB system can be improved by combining it with AMB [7], or superconducting bearings [8]. The damping property of the PMB can be improved using passive means such as viscoelastic dampers [9] or eddy current dampers [10]. Non-contact eddy current dampers are the best option to improve the damping properties of PMB. For a high-speed turbo compressor rotor, an eddy current damping system was developed [11]. With the help of Maxwell's equations, an analytical model for the damping force was developed. A mathematical model was established in [12] to identify the ECD properties when PMB supports rotors. In ECD, dynamic interactions between the eddy currents generated in the conductor and a moving magnetic field cause the generation of damping forces on the rotor. Modeling ECD for damping forces is a difficult task. In the recent past, both analytical methods and FEA simulations were adopted by researchers [14–16] to evaluate damping forces. In [16], the authors reported a 40% of error between the analytical and experimental results. Transient FEA can be used to analyze ECD. More accurate results can be obtained in FEA but at the cost of high computational time. In [15], researchers used the concept of curve fitting in FEA results along with the analytical results to calculate damping characteristics.

With the help of finite element software, single-objective problems have been solved. But they pose a problem of long computational time as well as the inability to obtain the optimal solution [13]. In [14–16], the optimization of magnetic bearings has been performed based on volume and suspension force as a single objective. Optimization yielded better results, but the bearing performance was reduced. In [17], a multi-objective genetic algorithm was used to optimize the hybrid magnetic bearing. Radial magnetic bearings [18] were optimized using particle swarm optimization with volume and loss as optimization objectives, and due to optimization, better results were obtained. A multi-objective genetic particle swarm optimization [13] was used in magnetic bearing. The results indicated that there was an 18% increase in suspension force, and a reduction in volume was 22%. In [19, 20], the authors presented a method for optimizing the bearing characteristics of axially and perpendicularly polarized multiring PM thrust bearings within a cylindrical volume. In addition to plotting the optimum thickness and inner diameters of each ring, generalized plots are provided regarding the outer diameter of the bearing. In [21], a comprehensive optimization technique for axially stacked radial PMBs was developed. Based on the given length and outer diameter of the stator, equations were given for calculating mean radius and clearance. For a stack radial passive magnetic bearing [22], multi-objective optimization was performed. Based on constraints, constants, and bounds of the literature, the authors presented the optimization results. In this paper, as the derived equations are three-dimensional semi-analytical, a discrete optimization process was adopted.

Considering the inaccuracy of analytical results for damping properties, in the present research,

electromagnetic transient finite element analysis is carried out to calculate damping properties for an optimized RMD permanent magnet thrust bearing. Analysis of the ECD system for an optimized RMD configuration in a given volume of magnet was not addressed by the researchers in the literature.

The major contributions of the present paper are: (1) presented the generalized mathematical equations for features of RMDPMTB, (2) the design and optimization of RMDPMTB in a particular volume of the magnet was carried out, (3) generalized the optimization procedure so as to express the critical design variables in the form of curve-fit equations, (4) the usage of curve-fit equations for optimization process using a generalized example of the bearing was demonstrated, and (5) the analysis of ECD for an optimized RMD permanent magnet thrust bearing was carried out for damping properties in ANSYS.

2. BEARING STRUCTURE WITH NON-CONTACT EDDY CURRENT DAMPER

A PMB with a single ring generates low force and stiffness as compared to the conventional bearing. Incorporating multiple rings, where rings in both the rotor and the stator are magnetized either axially or radially, produces comparable force and stiffness as traditional bearings. RMD structures employ axially and radially magnetized rings to enhance the force and stiffness further. Levitation occurs due to the magnetic forces generated between the faces of the rotor and stator. An RMD thrust bearing configuration with a copper plate in the rotor is shown in Fig. 1.

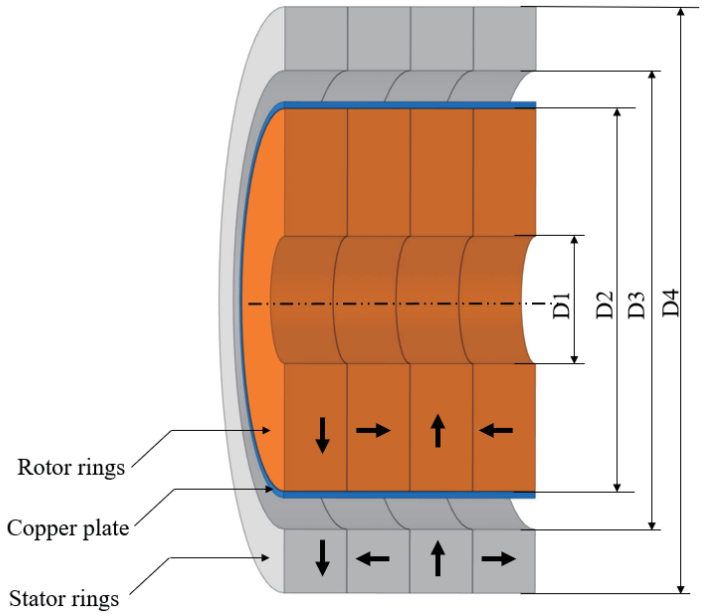

Figure 1. Structure of RMDPMTB.

3. MATHEMATICAL MODEL

In this section, a mathematical model for evaluating the bearing properties in RMDPMTB is presented. The outer rings exert a net force on inner rings due to interactions among (i) AxiallyAxially (ii) RadiallyRadially, and (iii) AxiallyRadially or RadiallyAxially polarized magnet rings. The magnetic interactions between the faces of axially and radially polarized rings are depicted in Fig. 2. Let the p^{th} ring be mounted on the rotor which is free to move with respect to the q^{th} ring mounted on the stator in the Cartesian coordinate system. Charged surfaces of magnet rings are denoted as 1, 2, 3, and 4 as shown in Fig. 2. The net axial force acting on the rotor rings as a result of interactions among all faces

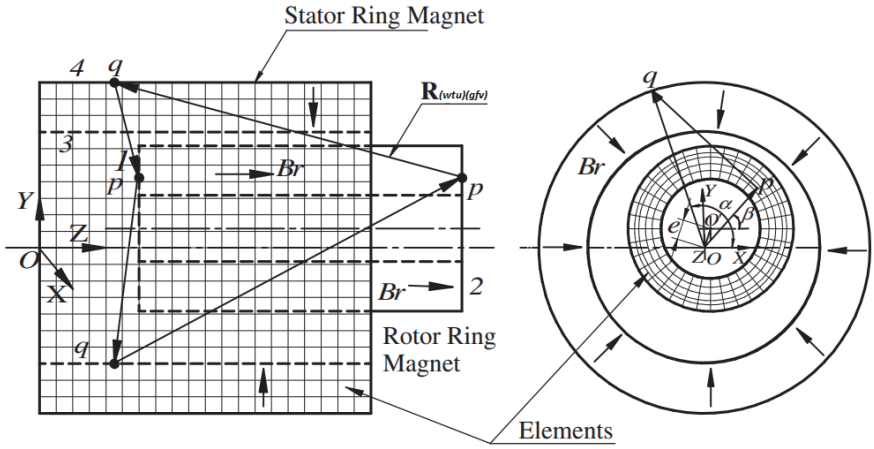

Figure 2. Interactions between axially and radially polarized magnet rings.

of stator-rotor rings is given by Equation (1).

$$F_z = \frac{B_r^2}{4\pi\mu_0} \sum_{p=1}^{n} \sum_{q=1}^{n} \sum_{t=1}^{2} \sum_{f=3}^{4} \sum_{w=1}^{m} \sum_{g=1}^{m} \frac{S_{wtp} S_{gfq}}{R^3_{(wtp)(gfq)}} R_{(wtp)(gfq)} \left(-1\right)^{(t+f)} \left(-1\right)^{(b)} \tag{1}$$

Discrete elements on the faces of magnet rings are m. The surface area of w^{th} element positioned on the t^{th} surface of the p^{th} rotor magnet is denoted as S_{wtp}, and S_{gfq} denotes the surface area of the g^{th} element positioned on the f^{th} surface of the q^{th} stator magnet.

$$\mathbf{R} = \sqrt{\left(X_{gfq} - X_{wtp}\right)^2 + \left(Y_{gfq} - Y_{wtp}\right)^2 + \left(Z_{gfq} - Z_{wtp}\right)^2}$$

and

$$R_{(wtp)(gfq)} = \left(X_{gfq} - X_{wtp}\right) i + \left(Y_{gfq} - Y_{wtp}\right) j + \left(Z_{gfq} - Z_{wtp}\right) k$$

The position coordinates of the elements of the faces are given below.

If p and q are odd values

$$\begin{aligned} X_{wtp} &= \left(x + r_{mr} \cos\beta\right) i & X_{gfq} &= \left(r_{ms} \cos\alpha\right) i \\ Y_{wtp} &= \left(y + r_{mr} \sin\beta\right) j & Y_{gfq} &= \left(r_{ms} \cos\alpha\right) j \\ Z_{wtp} &= \left(z + (u-1)l\right) k & Z_{gfq} &= \left(vl\right) k \end{aligned} \tag{2}$$

If p and q are even values

$$\begin{aligned} X_{wtp} &= \left(x + R2 \cos\beta\right) i & X_{gfq} &= \left(R4 \cos\alpha\right) i \\ Y_{wtp} &= \left(y + R2 \sin\beta\right) j & Y_{gfq} &= \left(R4 \sin\alpha\right) j \\ Z_{wtp} &= \left(z + l_m\right) k & Z_{gfq} &= \left(l_m\right) k \end{aligned} \tag{3}$$

$$l_m = l\left(h-1\right) + \left(j-1\right) \frac{1}{N_1} + \frac{1}{2N_1}$$

where h is either p or q, and p and $q = 1, 2, 3, \ldots n$. The surfaces of the polarized rings are divided into an $N1$ number of elements and $j = 1, 2, 3, \ldots N1$.

The following criteria are used to evaluate the value of b in Eq. (1).

If p is even or odd, and $(p+q)$ is even,

$$b = \left(\frac{(p+q)}{2} - p\right) \tag{4}$$

If p is even, and $(p+q)$ is odd

$$b = \left(\frac{(p+q+1)}{2} - p\right) \tag{5}$$

If p is odd, and $(p+q)$ is odd

$$b = \left(\frac{(p+q-1)}{2} - p\right) \tag{6}$$

The axial stiffness generated in RMDPMTB is given by

$$K_Z = -\frac{dF_z}{dZ} \tag{7}$$

By using MATLAB, the maximum force and stiffness are determined by employing Eqs. (1)–(7).

4. OPTIMIZATION OF RMDPMTB

This section provides designers with guidelines for sizing RMD thrust-bearing rings. The optimization of the important bearing characteristics was performed for a given volume of the bearing. The design and optimization procedure of RMDPMTB is explained in Fig. 3.

1. To start with, the dimensions of a monolithic thrust PMB, (n, g, Br, D_1, D_2, D_3, D_4, and L) were assumed.

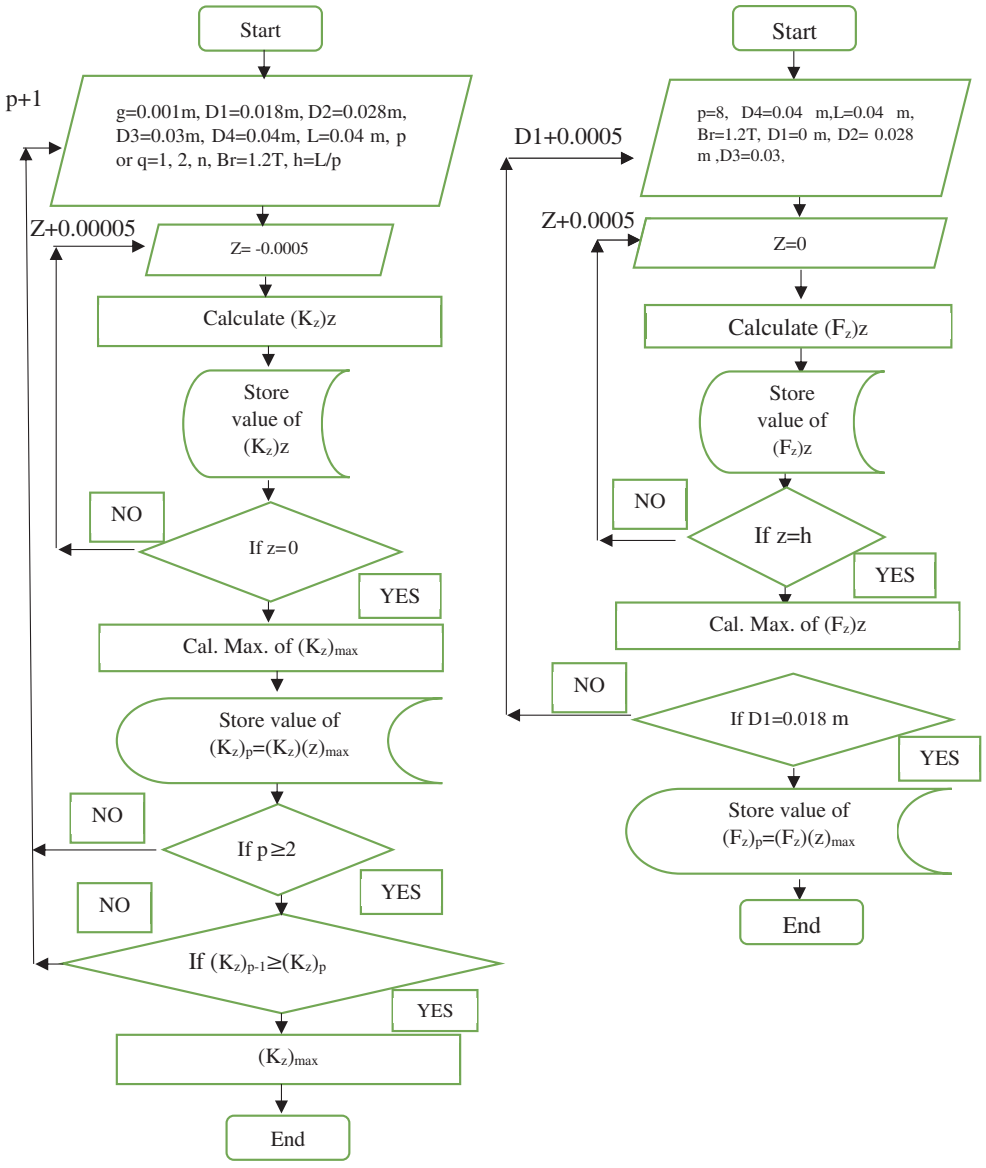

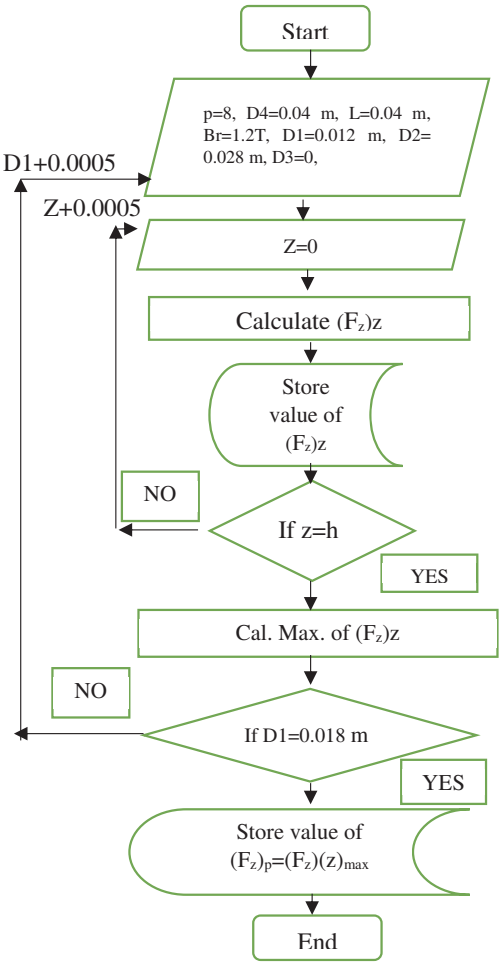

Figure 3. Flow charts of optimization process (a) optimization of number of rings for maximum stiffness (b) optimization of $D1$ for maximum force (c) optimization of $D3$ for maximum force.

2. Characteristics in RMD configuration are dependent on the axial position of the rotor. The values of axial positions for both force and stiffness are fixed initially for calculating the maximum characteristics. Eqs. (1) to (7) are used to calculate axial force and stiffness values in the bearing configuration.
3. Optimum values of number of ring magnets (n_{opt}) are calculated by varying the number of rings for the calculated range of axial offset values.
4. $D1$ is optimized for the selected value of air gap by utilizing the optimized values determined in steps (2) to (4).
5. Optimization of $D3$ is carried out at 'n_{opt}' and '$D1_{opt}$'.
6. Air gap values are varied from 0.25 to 2 mm in steps of 0.25 mm, and steps (2) to (5) are repeated.
7. The optimization is generalized by developing a relationship between optimum design variables (h_{opt}, $D1_{opt}$, and $D3_{opt}$) and the ratio ($g/D4$), and the corresponding curve fit equations with the nature of variations for all optimum design variables in RMDPMTB are shown in Figs. 4 to 8.

In Figs. 4 and 7, the thickness of the ring increases with an increase in air gap. For a certain value of the air gap, the rotor's inner diameter ($D1$) remains constant, and when there is an increase in air gap, the optimum value of $D1$ decreases suddenly (Figs. 5 and 8). The optimum value of shaft diameter decreases with increase in the air gap. In Figs. 6 and 9, the stator's inner diameter is constant for both force and stiffness.

5. DEMONSTRATION OF THE OPTIMIZATION PROCEDURE

This section aims to demonstrate an overall optimum design methodology that achieves maximum bearing features for thrust PMBs.

1. Ratios of (g/D_4 and L/D_4) can be chosen from the given values as follows: A ratio describes the space available around a shaft in a specific application, e.g., $g/D_4 = 0.025$ and $L/D_4 = 0.5$ are used in this work.

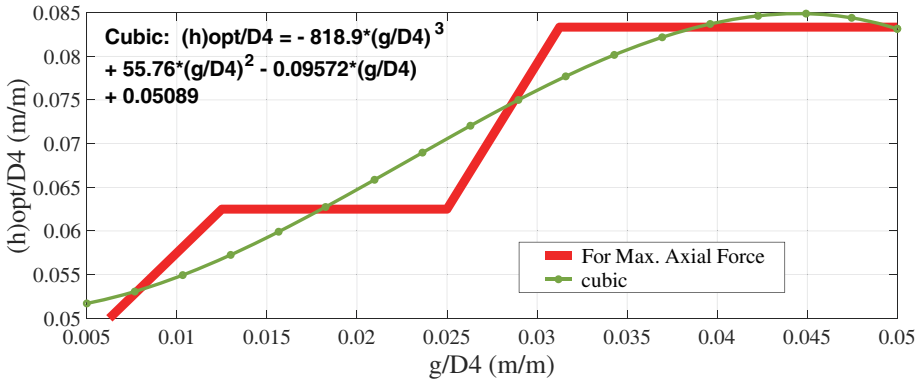

Figure 4. Curve fit equation for $n_{opt}(L/(h)_{opt})$ at $F_{z\,\max}$.

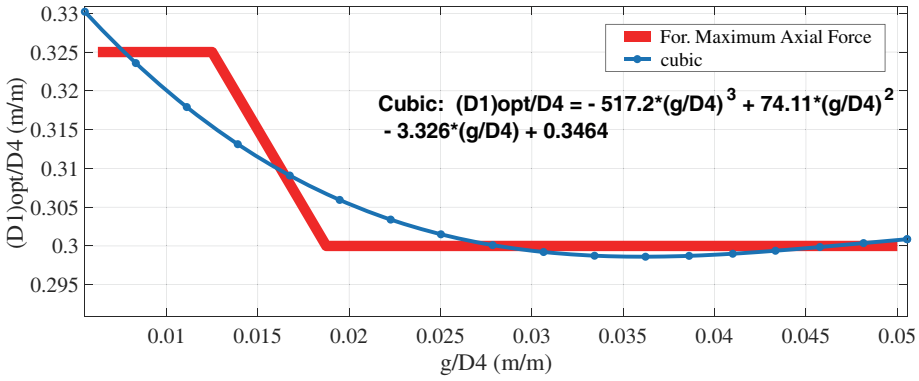

Figure 5. Curve fit equation for $(D_3)_{opt}$ at $F_{z\,\max}$.

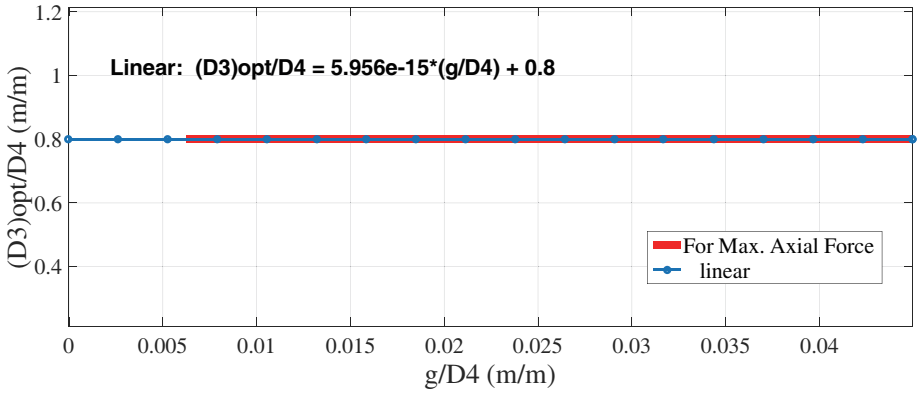

Figure 6. Curve fit equation for $(D_1)_{opt}$ at $F_{z\,\max}$.

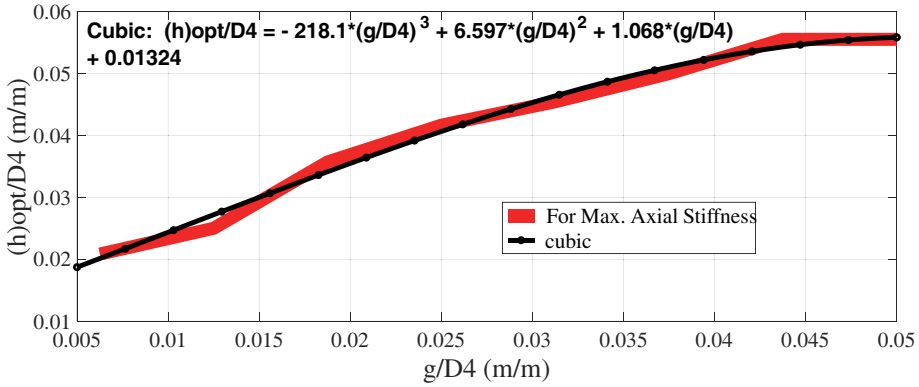

Figure 7. Curve fit equation for n_{opt} $(L/(h)_{opt})$ at $K_{z\,\max}$.

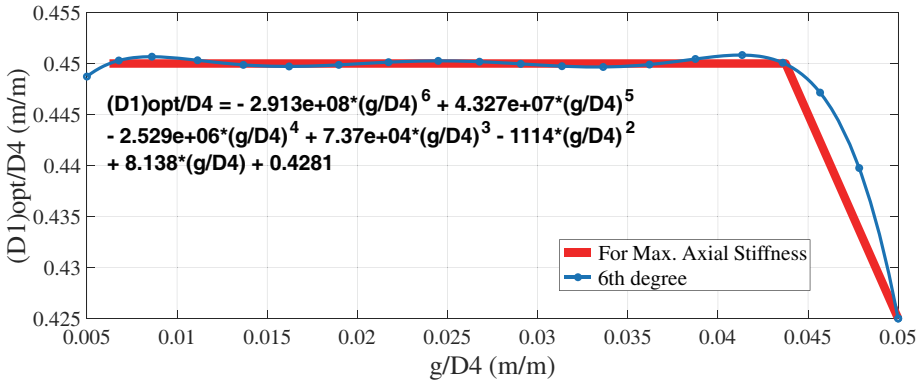

Figure 8. Curve fit equation for $(D_1)_{opt}$ at $K_{z\,\max}$.

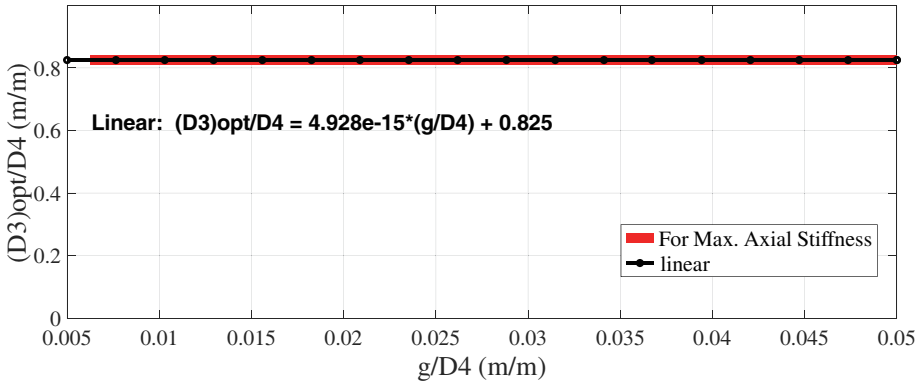

Figure 9. Curve fit equation for $(D_3)_{opt}$ at $K_{z\,\max}$.

2. It is important to choose the air gap value (g) based on the required force, stiffness, and size of magnet rings. $D_4 = 40\,\text{mm}$ and $L = 20$ are calculated, and $g = 1\,\text{mm}$.
3. Using curve fit plots, determine the best bearing design parameters (n, D_1, D_2, and D_3) for maximum F_Z and K_Z values. Optimized bearing dimensions are shown in Table 1 and Table 2.
4. The force calculation is computed using Eq. (1). Maximum stiffness is calculated by Eq. (7). By employing MATLAB, Eq. (1) and Eq. (7) are solved to ascertain axial force and maximum axial stiffness by utilizing optimized parameters obtained in Table 1 and Table 2. An axial force was

also calculated by creating a model in ANSYS mechanical APDL using optimized geometrical parameters, and the result is shown in Table 1. A deviation of 1.41% exists between the force values computed using the proposed optimization method and those determined using ANSYS.

Table 1. Optimized design variables at $F_{z\max}$.

For D_4 = 40 mm, g/D_4 = 0.025 as well as L/ D_4 = 0.5,		
Variables	**Equations**	**Variables Optimum Values**
$\mathbf{h_o}$	$\frac{h_o}{D_4} = -819 \times \left(\frac{g}{D_4}\right)^3 + 55.8 \times \left(\frac{g}{D_4}\right)^2 - 0.0957 \times \left(\frac{g}{D_4}\right) + 0.0509$	h_o = thickness of rings=2.82, n_0 = 8
$\mathbf{D_{1\ opt}}$	$\left(\frac{D_1}{D_4}\right) = -517.2 \times \left(\frac{g}{D_4}\right)^3 + 74.11 \times \left(\frac{g}{D_4}\right)^2 - 3.326 \times \left(\frac{g}{D_4}\right) + 0.3464$	$D_{1\ opt}$ = 12
$\mathbf{D_{3\ opt}}$	$\left(\frac{D_1}{D_4}\right) = 5.956 \times 10^{-15} \times \left(\frac{g}{D_4}\right) + 0.8$	$D_{3\ opt}$ = 32
$\mathbf{D_{2\ opt}}$	$D_{2\ opt} = D_{3\ opt} - 2g$	$D_{2\ opt}$ = 30
$\mathbf{F_{zmax}}$	Maximum axial force (Optimization)	771.49 N
$\mathbf{F_{zmax}}$	Maximum axial force (using ANSYS)	782.55 N
	% of deviation	1.41

Table 2. Optimized design variables at $K_{z\max}$.

For D_4 = 40 mm, g/ D_4 = 0.025 and L/ D_4 = 0.5,		
Variables	**Equations**	**Variables Optimum Values**
$\mathbf{h_o}$	$\frac{h_o}{D_4} = -218.1 \times \left(\frac{g}{D_4}\right)^3 + 6.597 \times \left(\frac{g}{D_4}\right)^2 + 1.068 \times \left(\frac{g}{D_4}\right) + 0.01324$	h_o = 1.62 n_0 = 12
$\mathbf{D_{1\ opt}}$	$\left(\frac{D_1}{D_4}\right) = -2.913 \times 10^8 \times \left(\frac{g}{D_4}\right)^6 + 4.327 \times 10^7 \times \left(\frac{g}{D_4}\right)^5 - 2.529 \times 10^6 \times \left(\frac{g}{D_4}\right)^4 + 7.37 \times 10^4 \times \left(\frac{g}{D_4}\right)^3 - 1114 \times \left(\frac{g}{D_4}\right)^2 + 8.138 \times \left(\frac{g}{D_4}\right) + 0.4281$	$D_{1\ opt}$ = 18 mm
$\mathbf{D_{3\ opt}}$	$\left(\frac{D_1}{D_4}\right) = 4.928 \times 10^{-15} \times \left(\frac{g}{D_4}\right) + 0.825$	$D_{3\ opt}$ = 33 mm
$\mathbf{D_{2\ opt}}$	$D_{2\ opt} = D_{3\ opt} - 2g$	$D_{2\ opt}$ = 31 mm
$\mathbf{K_{zmax}}$	Maximum axial stiffness	588737.2 N/mm

6. ANALYSIS OF DAMPING SYSTEM

The damping of the PMB is improved by inserting a cylindrical copper plate into the rotor of the optimized thrust bearing. When the bearing's rotor rotates, eddy currents are induced in the copper ring as a result of the interaction of the stator's magnetic fields, and a Lorentz force is generated, which exerts a force on the plate. The whole bearing geometry was modeled using the SOLID97 element of the ANSYS APDL, and coercive force values corresponding to grades of NdFeB magnets were used to polarize the rings in the axial (z-axis) and radial directions (x-axis) using an orthotropic material properties section in ANSYS. It is generally possible to obtain a stable magnetic field for permanent magnets by utilizing two-step loading in the case of transient analysis, as shown in Fig. 10. Initially, the magnetic flux increases, then remains constant in the second step.

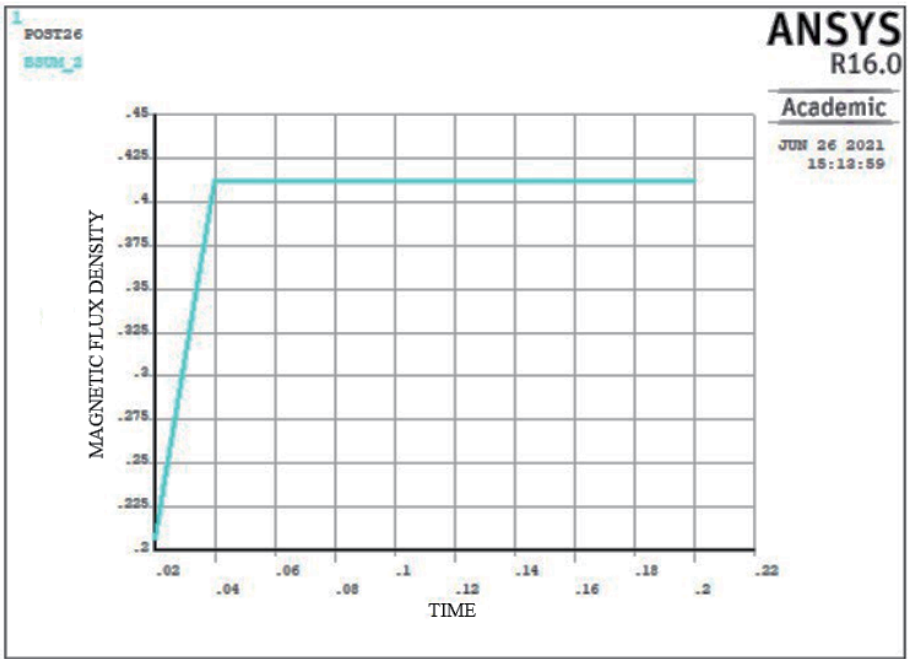

Figure 10. Magnetic flux density vs time.

To achieve optimum axial force, the rotor rings are spaced 2.5 mm apart from the stator rings for a configuration with maximum axial force. There is no offset between the rotor and stator for a configuration with maximum axial stiffness.

Finite element analysis has been performed for the rotor's axial and radial speeds. For both configurations, speeds are changed from 0 to 50 m/s in steps of 5 m/s. The material properties for a configuration with maximum axial force are given in Table 3, and those with the maximum stiffness are given in Table 4.

The variation of the axial, radial, and rotational damping forces for the configuration generating maximum axial force are shown in Fig. 11. Increasing speed causes the axial damping force to increase

Table 3. Material properties for a configuration having maximum axial force.

Sl. No	Material	Relative permeability	Resistivity (Ωm)	Dimensions
1	$N35$, $Br = 1.2\,\mathrm{T}$	1.1	1.8×10^{-6}	$D_1 = 12\,\mathrm{mm}$, $D_2 = 30\,\mathrm{mm}$, $D_3 = 32\,\mathrm{mm}$, $D_4 = 40\,\mathrm{mm}$, $n = 8$
2	Copper	1	1.72×10^{-8}	Thickness, $t = 0.5\,\mathrm{mm}$

Table 4. Material properties for a configuration having maximum axial stiffness.

Sl. No	Material	Relative permeability	Resistivity (Ωm)	Dimensions
1	$N35$, $Br = 1.2\,\mathrm{T}$	1.1	1.8×10^{-6}	$D1 = 18\,\mathrm{mm}$, $D2 = 31\,\mathrm{mm}$, $D3 = 33\,\mathrm{mm}$, $D4 = 40\,\mathrm{mm}$, $n = 12$
2	Copper	1	1.72×10^{-8}	Thickness, $t = 0.5\,\mathrm{mm}$

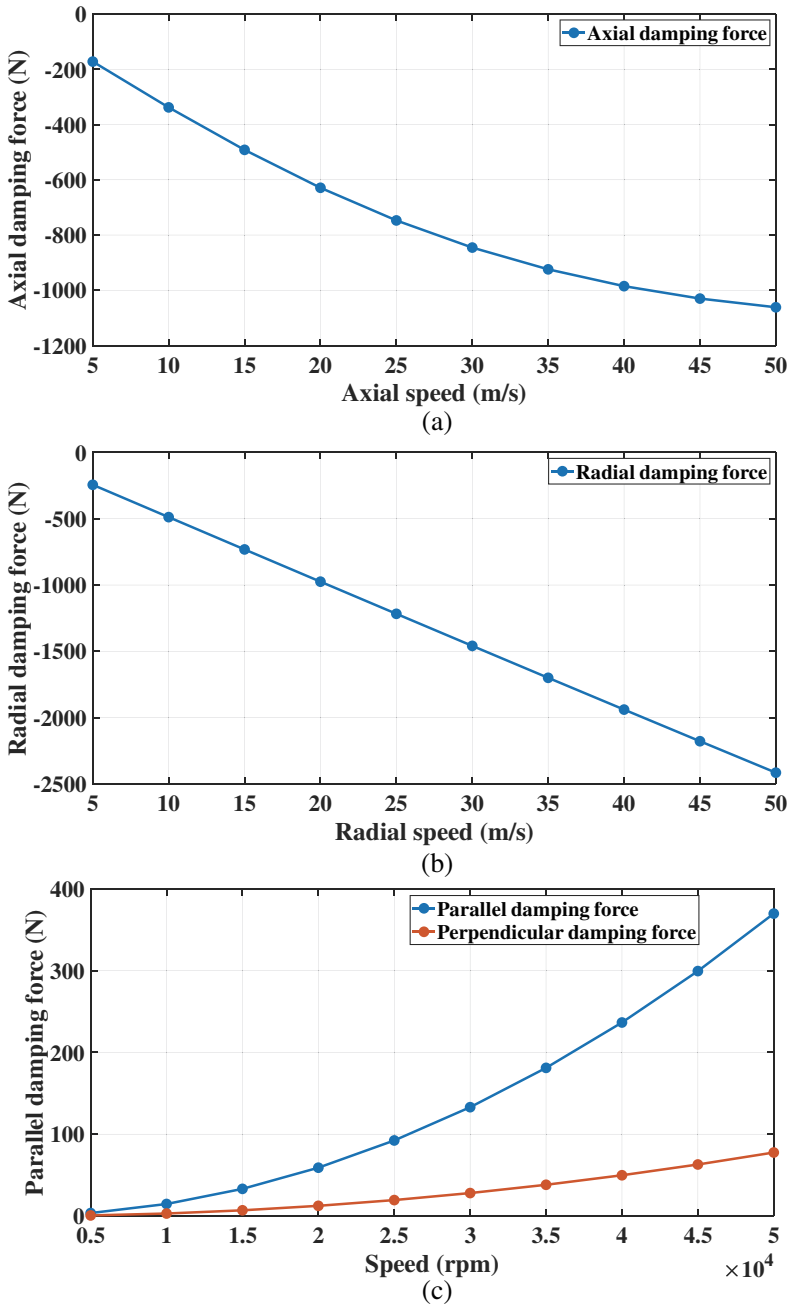

Figure 11. Results of RMDPMTB at $F_{z\,\max}$ (a) axial damping force, (b) radial damping force, (c) rotational damping force.

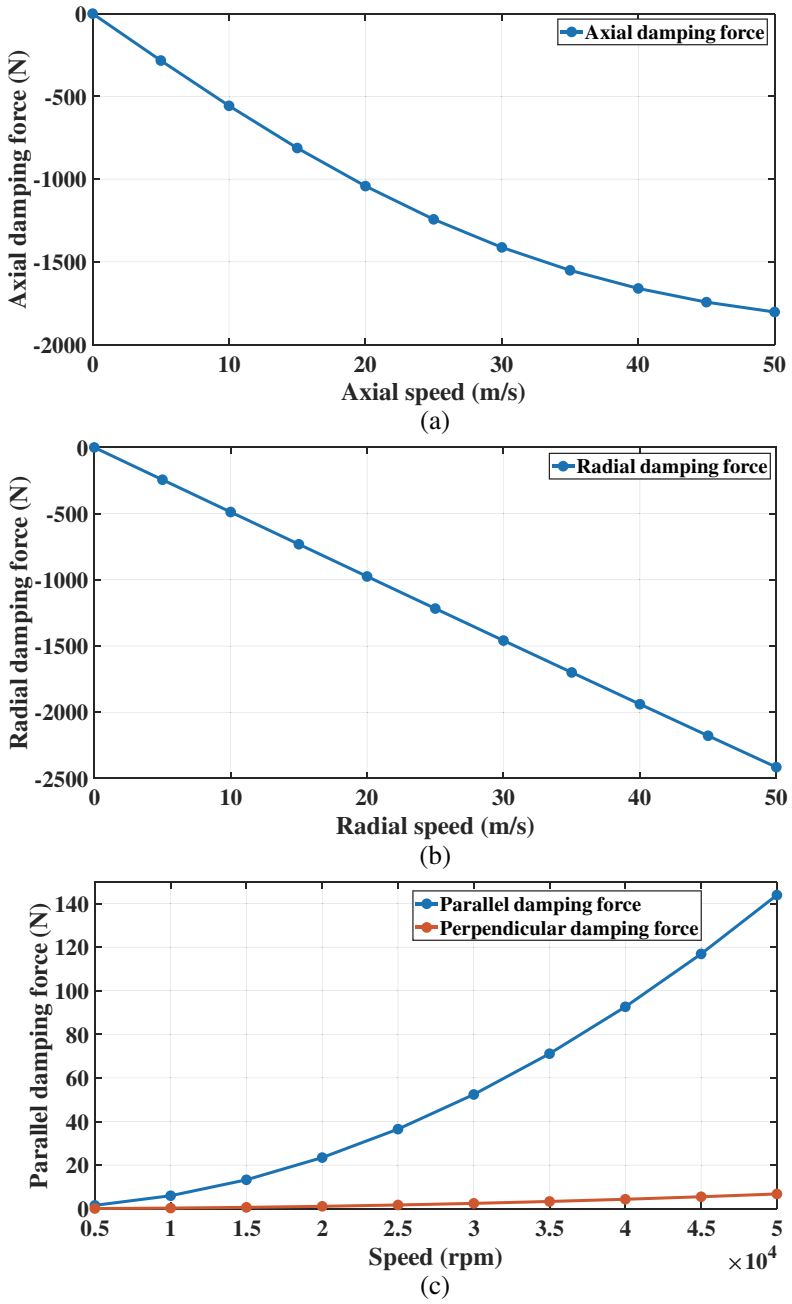

Figure 12. Results of RMDPMTB at $K_{z\max}$ (a) axial damping force, (b) radial damping force, (c) rotational damping force.

and almost become constant. In contrast, radial damping force increases linearly when speed is increased.

Figure 12 shows the variation of the axial, radial, and rotating damping forces for the configuration generating maximum stiffness. With an increase in axial speed, the corresponding damping force increases and will become constant. Alternatively, radial damping force increases linearly as speed increases. Based on these observations, it is evident that rotation speed increases induced eddy current, resulting in increased damping force.

Damping forces are computed for various thicknesses of the copper plate for both configurations at the speeds where damping forces are maximum. When the thickness of the copper plate increases,

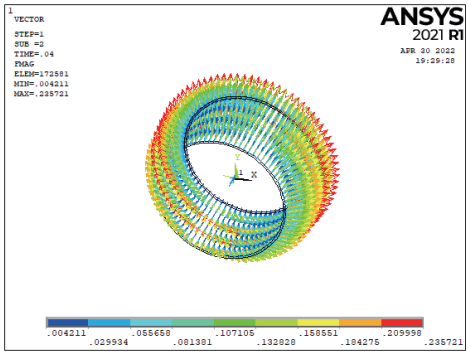

Figure 13. Eddy current distribution at an axial speed of 20 m/s.

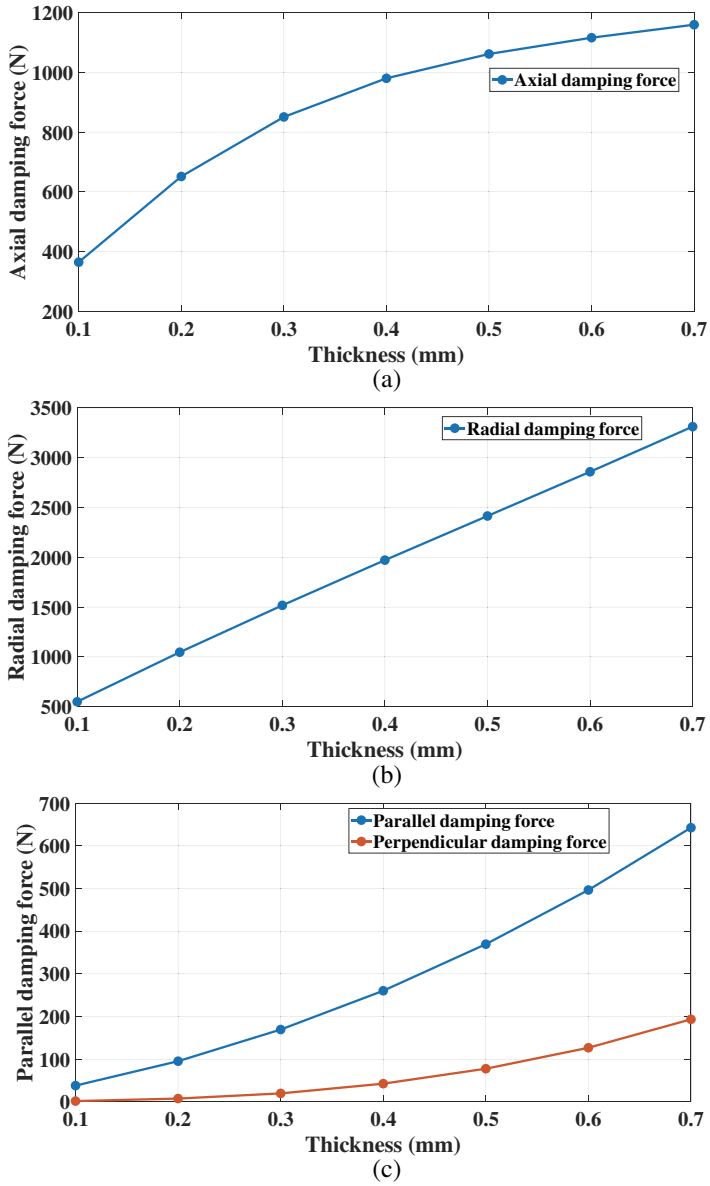

Figure 14. Results of damping force (a) axial, (b) radial, (c) rotational Vs. conductor plate thickness in RMDPMTB at $F_{z\max}$.

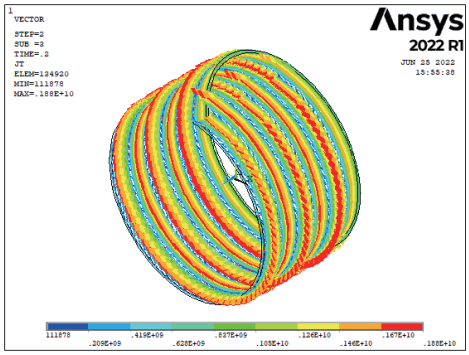

Figure 15. Eddy current distribution at radial speed of 20 m/s.

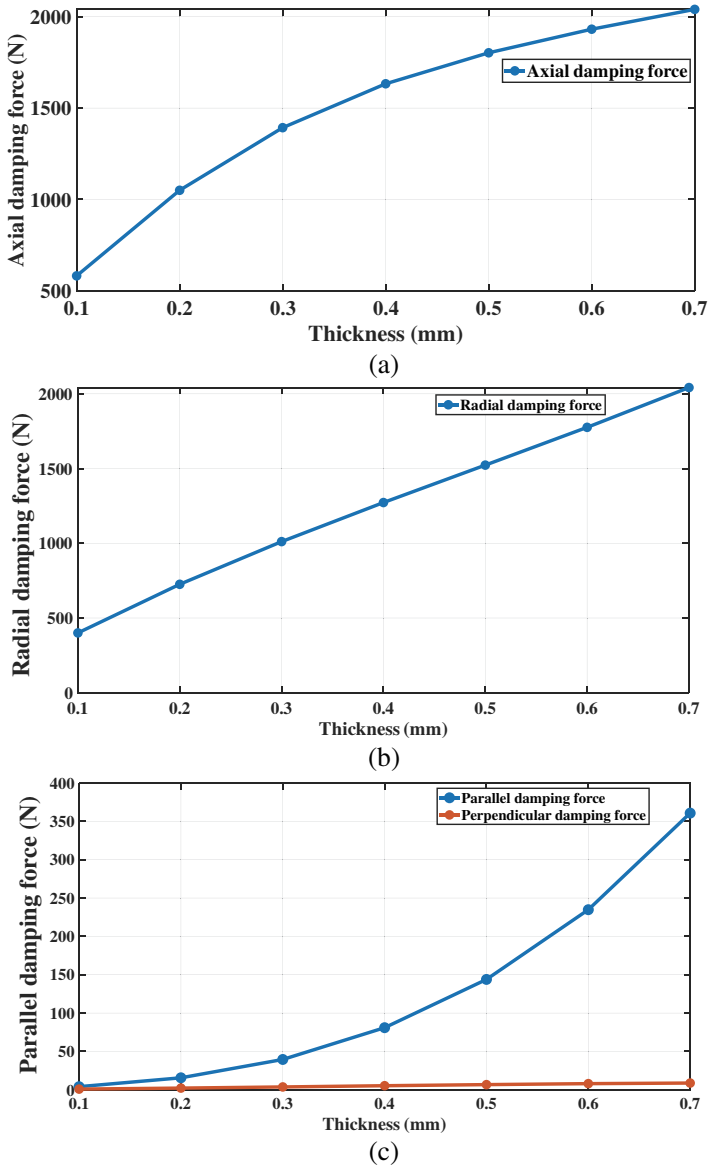

Figure 16. Results of damping force (a) axial, (b) radial (c) rotational Vs. conductor plate thickness in RMDPMTB at $K_{z\,\max}$.

the axial damping force rises gradually. In the case of radial damping force, it increases linearly. In comparison, parallel and perpendicular damping forces keep increasing with the increase in thickness of the copper plate which can be seen in Fig. 14 and Fig. 16 for both configurations.

The eddy current distributions for the two configurations are shown in Figs. 13 and 15. The red colour indicates an increase in current density near the magnet surface. The current density decreases inside the material.

7. CONCLUSIONS

Optimization of the RMDPMTB is carried out in a particular volume of a magnet (defined by $D4$ and L). Curve fit equations representing the optimum design variables were used to optimize the RMDPMTB for maximum characteristics. In industry, the designer can directly use the generalized curve fit equations of the optimum design variables for designing and optimizing RMD configuration. The damping force generated is dependent upon the rotor speed. The higher the speed, the greater the damping force. The RMD thrust bearing with maximum stiffness gave a much higher damping force than the configuration with maximum axial force. Damping force is dependent upon the thickness of the copper plate.

REFERENCES

1. Maslen, E. H. and G. Schweitzer, Eds., *Magnetic Bearings*, Springer Berlin Heidelberg, Vol. 53, No. 9, Berlin, Heidelberg, 2009.
2. Bleuler, H., et al., *Magnetic Bearings*, Springer Berlin Heidelberg, Berlin, Heidelberg, 2009.
3. Tian, L., X. P. Ai, and Y. Q. Tian, "Analytical model of magnetic force for axial stack permanentmagnet bearings," *IEEE Trans. Magn.*, Vol. 48, No. 10, 2592–2599, 2012.
4. Marth, E., G. Jungmayr, and W. Amrhein, "A 2-D-based analytical method for calculating permanent magnetic ring bearings with arbitrary magnetisation and its application to optimal bearing design," *IEEE Trans. Magn.*, Vol. 50, No. 5, 1–8, 2014.
5. Bekinal, S. I., M. Doddamani, and N. D. Dravid, "Utilization of low computational cost two dimensional analytical equations in optimization of multi rings permanent magnet thrust bearings," *Progress In Electromagnetics Research M*, Vol. 62, 51–63, 2017.
6. Bekinal, S. I. and S. Jana, "Generalized three-dimensional mathematical models for force and stiffness in axially, radially, and perpendicularly magnetized passive magnetic bearings with 'n' number of ring pairs," *J. Tribol.*, Vol. 138, No. 3, 1–9, 2016.
7. Sodano, H. A. and D. J. Inman, "Modelling of a new active eddy current vibration control system," *J. Dyn. Syst. Meas. Control. Trans. ASME*, Vol. 130, No. 2, 0210091–02100911, 2008.
8. Supreeth, D. K., S. I. Bekinal, S. R. Chandranna, and M. Doddamani, "A review of superconducting magnetic bearings and their application," *IEEE Trans. Appl. Supercond.*, Vol. 32, No. 3, 3800215, 2022.
9. Passenbrunner, J., G. Jungmayr, and W. Amrhein, "Design and analysis of a 1D actively stabilized system with viscoelastic damping support," *Actuators*, Vol. 8, No. 2, 1–18, 2019.
10. Deshwal, D., S. I. Bekinal, and M. Doddamani, "Analysis of novel eddy current damper for multi-ring permanent magnet thrust bearing," *Progress In Electromagnetics Research M*, Vol. 104, 13–22, 2021.
11. Fang, Y. Le, J. Sun, and K. Wang, "Analysis and design of passive magnetic bearing and damping system for high-speed compressor," *IEEE Trans. Magn.*, Vol. 48, No. 9, 2528–2537, 2012.
12. Detoni, J. G., Q. Cui, N. Amati, and A. Tonoli, "Modelling and evaluation of damping coefficient of eddy current dampers in rotordynamic applications," *J. Sound Vib.*, Vol. 373, 52–65, 2016.
13. Sun, Y., S. Yin, Y. Yuan, Y. Huang, and F. Yang, "Multi-objective optimization design of magnetic bearing based on genetic particle swarm optimization," *Progress In Electromagnetics Research M*, Vol. 81, 181–192, 2019.

14. Moser, R., J. Sandtner, and H. Bleuler, "Optimization of repulsive passive magnetic bearings," *IEEE Trans. Magn.*, Vol. 42, No. 8, 2038–2042, 2006.
15. Zeisberger, M., T. Habisreuther, D. Litzkendorf, O. Surzhenko, R. Muller, and W. Gawalek, "Optimization of levitation forces," *IEEE Trans. Appiled Supercond.*, Vol. 11, No. 1, 1741–1744, Mar. 2001.
16. Sahinkaya, M. N. and A. E. Hartavi, "Variable bias current in magnetic bearings for energy optimization," *IEEE Trans. Magn.*, Vol. 43, No. 3, 1052–1060, 2007.
17. Rao, J. S. and R. Tiwari, "Optimum design and analysis of axial hybrid magnetic bearings using multi-objective genetic algorithms," *Int. J. Comput. Methods Eng. Sci. Mech.*, Vol. 13, No. 1, 10–27, 2012.
18. Liu, X. and B. Han, "The multiobjective optimal design of a two-degree-of-freedom hybrid magnetic bearing," *IEEE Trans. Magn.*, Vol. 50, No. 9, 2014.
19. Bekinal, S. I., M. Doddamani, and S. Jana, "Optimization of axially magnetized stack structured permanent magnet thrust bearing using three-dimensional mathematical model," *J. Tribol.*, Vol. 139, No. 3, 1–9, 2017.
20. Bekinal, S. I., M. Doddamani, M. Vanarotti, and S. Jana, "Generalized optimization procedure for rotational magnetized direction permanent magnet thrust bearing configuration," *Proc. Inst. Mech. Eng. Part C J. Mech. Eng. Sci.*, Vol. 233, No. 7, 2563–2573, 2019.
21. Lijesh, K. P. M. Doddamani, and S. I. Bekinal, "A pragmatic optimization of axial stack-radial passive magnetic bearings," *J. Tribol.*, Vol. 140, No. 2, 1–9, 2018.
22. Lijesh, K. P., M. Doddamani, S. I. Bekinal, and S. M. Muzakkir, "Multi-objective optimization of stacked radial passive magnetic bearing," *Proc. Inst. Mech. Eng. Part J J. Eng. Tribol.*, Vol. 232, No. 9, 1140–1159, 2018.